Available online at www.sciencedirect.com
SCIENCE DIRECT®
Journal of Catalysis 225 (2004) 78–85
JOURNAL OF CATALYSIS
www.elsevier.com/locate/jcat

Nanostructuring of binary molybdenum oxide catalysts for propene oxidation

J.B. Wagner,[a,*] S.B. Abd Hamid,[b] D. Othman,[b] O. Timpe,[a] S. Knobl,[a] D. Niemeyer,[a] D.S. Su,[a] and R. Schlögl [a]

[a] *Fritz-Haber Institut der MPG, Abteilung AC, Faradayweg 4-6, 14195 Berlin, Germany*
[b] *Combinatorial Technology and Catalysis Research Centre (COMBICAT), Universiti Malaya, 50603 Kuala Lumpur, Malaysia*

Received 6 January 2004; revised 23 March 2004; accepted 31 March 2004
Available online 24 April 2004

Abstract

Binary molybdenum oxides are active catalysts for propene oxidation to acrolein if they are structurally different from orthorhombic MoO_3 (o-Mo). The periodical structure of the as-synthesized precatalyst must be different from o-Mo to create the activity. Additional features typical for efficient catalysts are a bulk nanostructuring and a complex surface termination that are detectable in TEM examinations only. After transition into defective o-Mo the samples exhibit much reduced activities. The implications of these findings on the functional analysis of complex selective oxidation catalysts are discussed.

Keywords: Selective oxidation; Propene; Molybdenum oxides; TEM; Defect structures; Phase transformation

1. Introduction

The function of multielement multimetal oxide (MMO) catalysts based on molybdenum is a central research topic in the endeavor to understand and master the challenge of small alkane molecule activation. Actual systems such as molybdenum–vanadium–tellurium–niobium oxides (MOVTE) [1–4] or Mo–V–W [5] oxides contain several phases that are believed to be essential in their cooperation for proper function. Bulk o-Mo is described to be fully inactive [6,7] in alkane and olefin oxidation unless doped with another cation such as Sb, Bi, or V [8].

Supported Mo-oxide in the form of small aggregates known to contain both octahedral and tetrahedral building blocks are, however, active in alkane and olefin activation [9–11]. This and the fact that the majority of all selective oxidation catalysts contain Mo prompted us to reinvestigate the issue about the inactivity of molybdenum oxide. The target of such a study should be confirmation of the essential presence of a second cation other than Mo to achieve selective oxidation activity. In several reports it is stated that pure molybdenum oxide should be detrimental for the selective catalytic action of the rest of the MMO mixture posing the question after the selectivity of a possible catalytic activity of a single-phase molybdenum oxide [12]. Other studies find a high selectivity toward total oxidation with pure o-Mo samples [13].

Close inspection of the literature revealed that o-Mo was obtained by a high-temperature calcination of various precursors [6,7]. It should be noted that by precipitation binary o-Mo cannot be synthesized as primary product. A mixture of molybdenum oxide hydrates, of hexagonal MoO_3, and of a family of supramolecular oxo clusters familiar in synthetic inorganic chemistry [14–16] are the primary products. We have recently studied the conditions and selection mechanisms that allow controlling the species obtained by aqueous precipitation [17]. There is strong evidence from in situ studies that o-Mo is an active catalyst if it is suitably defected. Using time-resolved X-ray absorption spectroscopy coupled to pulse-response techniques it was possible to link the selective oxidation activity to the occurrence of lattice defects and to the beginning self-diffusivity of oxygen in o-Mo [18–20]. It is thus plausible that molybdenum oxides that carry the structural features of "defects" in their structural motif may be active catalysts in their own right and that the admixture of additional cations is at least a means of struc-

* Corresponding author.
E-mail address: wagner_j@fhi-berlin.mpg.de (J.B. Wagner).

0021-9517/$ – see front matter
doi:10.1016/j.jcat.2004.03.041

tural promotion helping to create/stabilize the defective state of o-Mo. Noncalcined phase-pure molybdenum oxides with structures different from o-Mo were synthesized and studied with respect to their catalytic action using temperature-programmed reaction spectroscopy (TPRS) of propene to separate intrinsic activity from activation–deactivation effects superimposed in conventional steady-state experiments and with transmission electron microscopy (TEM) in order to study the local ordering not detected by powder X-ray diffraction (XRD).

2. Experimental

2.1. Synthesis

Two prototype catalysts 1 and 2 were obtained in 100-g quantities using the controlled precipitation reactor described elsewhere [21]. Briefly, a stirred 4l reactor is equipped with computer-controlled pump systems and a monitoring system for pH and conductivity, allowing isothermal precipitation reactions to be conducted with time, pH, or conductivity as control variable, as described by Abd Hamid et al. [17]. The samples here were obtained in the decreasing pH mode using 0.5 M ammonium heptamolybdate (AHM) for sample 1 and 0.2 M AHM for sample 2 and 1 M HNO_3 as precipitation agent. Precipitation temperature was 323 K and the speed of addition was 40 ml/min. Fig. 1 shows the decrease of pH during the addition of HNO_3 for sample 1 and sample 2. The precipitate was dried without aging and washing at ambient temperature in a vacuum desiccator. The colorless samples exposing both 1.0 m^2/g BET surface area were used for all experiment without further treatment.

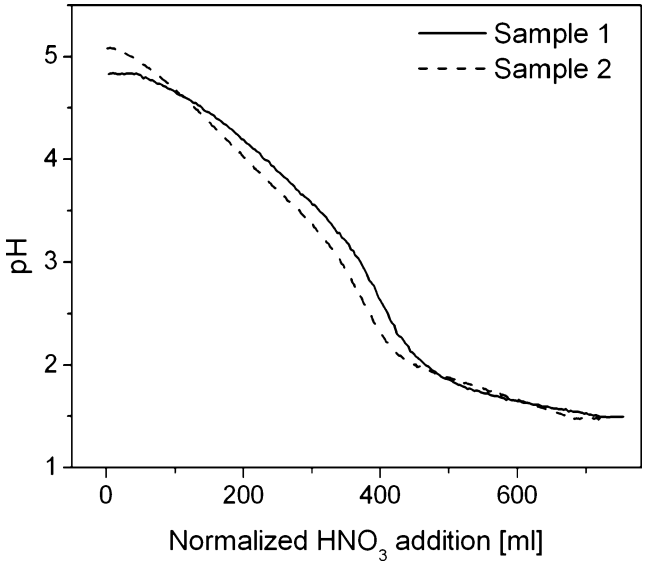

Fig. 1. pH response curves for sample 1 and sample 2 during addition of HNO_3.

2.2. Temperature-programmed reaction spectroscopy (TPRS)

A 6-mm quartz reactor was used to hold 50 mg of catalyst between beds of SiC. Feed gas of stoichiometric oxygen to propene mixture at a flow rate of 10 ml/min was applied. Samples were studied with linear heating ramps of 5 K/min in cycle including heating to 773 K, holding for 1 h, cooling down in feed to 400 K, and reheating to 773 K. A calibrated Balzers Omnistar quadrupole MS was used for gas analysis.

2.3. Structure analysis

Standard XRD patterns of the as-prepared samples were obtained in reflection geometry using a STOE diffractometer with scintillation counting.

TEM studies were conducted in a Philips CM 200 FEG instrument operated at 200 kV equipped with a Gatan Image Filter (GIF) and a CCD camera. The specimens were studied by dry dispersing the powder samples on standard copper grids coated with holey carbon film. This creates a propensity toward examining thin and small objects that contribute, however, most to the material relevant for catalytic function considering the small surface area and the nonporous nature of the systems.

3. Results

3.1. Catalytic activity

Both samples revealed catalytic activity toward partial and total oxidation without prior calcination. The conversion was kept to about 2% for both samples. The temperature profiles of Fig. 2A indicate that the different structures of samples 1 and 2 exhibit a quite pronounced influence on the evolution of the catalytic function. Sample 1 develops activity at 640 K in a temperature range well compatible with MMO systems whereas sample 2 requires a 700 K temperature, more typical for singly promoted bulk o-Mo. The selectivity to partial oxidation is also different as seen from the data in Fig. 2B. In both cases some initial evolution of CO_2 can be seen: for sample 1 some slight prereduction of the as-prepared oxide is observed at approx 540 K as produced CO_2 without consumption of gaseous O_2 (not shown here) whereas with sample 2 there is a pronounced extra peak superimposed on the leading edge of activity. The as-prepared oxide requires prereduction to become active. This was also noted with in situ XAS experiments where an onset temperature of 658 K was determined for defected o-Mo [19], which is in between the two temperatures found here.

The activity during the reheat treatments is shown in Fig. 2C, which reveals that both samples undergo an irreversible structural transformation leaving behind a less active material that does not remember its initial structural difference. This transformation does not occur in time scales of

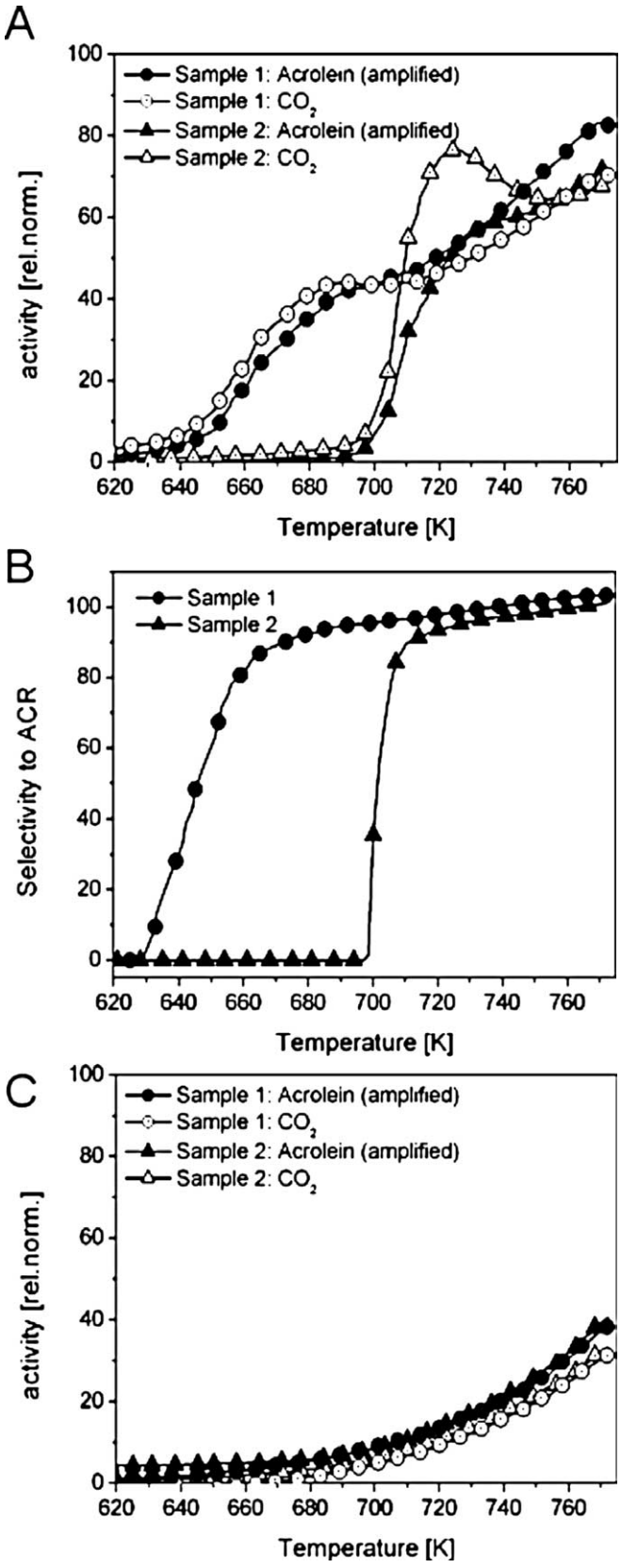

Fig. 2. Catalytic data on the studied samples. (A) Catalytic activity of the two samples under propene oxidation to CO_2 and acrolein. (B) Selectivity to acrolein of the studied samples under propene oxidation. (C) Activity of acrolein and CO_2 production under the second run of propene oxidation.

the TPRS experiment if the temperature is not cycled above 723 K. The samples remain stable in the high-temperature structure and deliver reproducible temperature vs activity profiles. In their low-temperature structures the samples also remain stable under the present testing conditions of low conversion, low load, and dry gas.

3.2. Average structures

Fig. 3 compares the powder X-ray diffraction patterns and the compilation of a large number of lattice fringe TEM images analysed by fast Fourier transform (FFT) for the two samples. Sample 1 exhibits an XRD of a supramolecular compound reminiscent of that from polyoxometallates (HPA) [22,23] with intense lines for a large unit cell and a family of weak reflections arising from the objects filling the large unit cell. Little can be said about the phase purity of such a material as the many lines at small $1/d$ values may arise from a low symmetry of a (hydrated) supramolecular phase or a mixture of several hydration stages of the same nonaqueous supramolecular structure [24]. This is frequently observed with HPA materials [25]. Sample 2

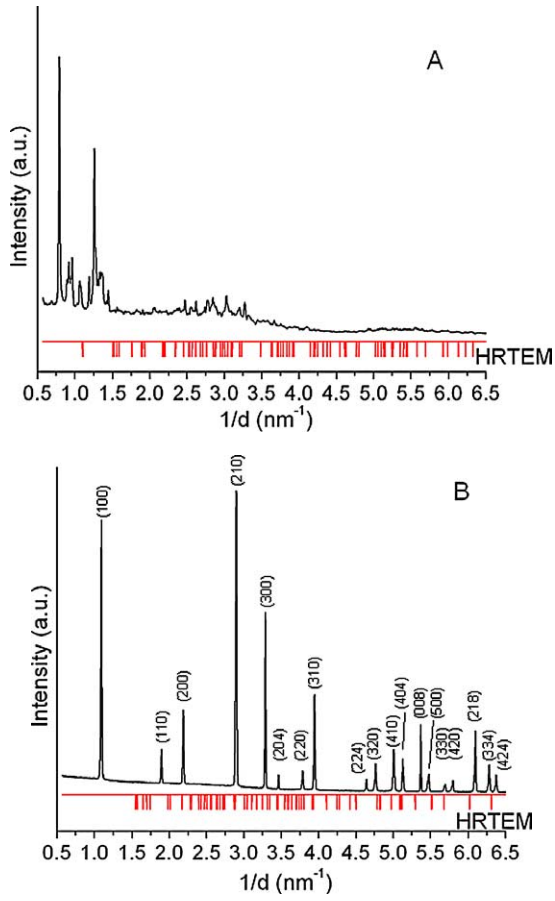

Fig. 3. X-ray diffraction patterns compared with lattice spacings revealed from a large number of lattice fringe TEM images (HRTEM). (A) Sample 1, (B) sample 2. The HRTEM analysis must be considered qualitatively.

exhibits the diffraction pattern of hexagonal MoO_3 (hex) [26].

It is highly significant that for both samples there are significant differences between the X-ray diffraction data and the data obtained by FFT from lattice fringe TEM images. This is not due to different structure factors for the two diffraction methods as model calculations for supramolecular Mo and hex-Mo clearly reveal. However it should be pointed out that HRTEM imaging cannot and should not be used quantitatively and thereby is performed qualitatively in the following.

The part of the material that is amenable to lattice fringe imaging is of a different structure in the two samples but also of a different structure than the large body of thick crystals contributing mainly to the XRD signals. No unique match was obtained between the *d*-spacings from lattice fringe images and the mutual angles with known binary and hydrated oxides. In sample 2 there seems to be some similarity of frequent lattice images with spacings close to those expected from the XRD hex phase but the agreement between the whole patterns is still much poorer than the error bar of the calibration for the lattice fringe images. The only conclusion at this point is that the samples are microheterogeneous and are in the form of small particles, materials that are different from known Mo oxides and also different from the structure of the large crystals in the sample.

3.3. Local structure as revealed by TEM

TEM and high-resolution TEM of the as-prepared samples 1 and 2 are used to investigate the local structural details, which are not explored by diffraction techniques. The relevance of this nanoscopic dimension for oxidation catalysts was elucidated recently with the Mo–V system [5].

SEM reveals that both materials consist of a large fraction of needle-like agglomerates and a small fraction of tiny objects. Characteristic images of the agglomerates are displayed in Fig. 4. Sample 1 (Fig. 4A) is typically more lamellae type and larger than the more regular shaped needles in sample 2 (Fig. 4B). EDX confirmed for both samples the absence of impurities to the detection level in large and small objects.

TEM inspection of the material from sample 1 reveals a different morphology as judged from the images of Fig. 5. Platelets with compact or porous inner structure are the typical shape of the thin objects besides the lamellae seen in Fig. 4. High magnification images of sample 1 reveal a high diversion in the crystalline structure of the sample. Thicker areas which a still transparent for the electron beam exhibit both amorphous areas as shown in Fig. 6A and single crystals sized up to 50 nm as seen in Fig. 6B. The lattice fringes revealed in Fig. 6B indicate a high ordering, but a unique determination of the structure cannot be determined

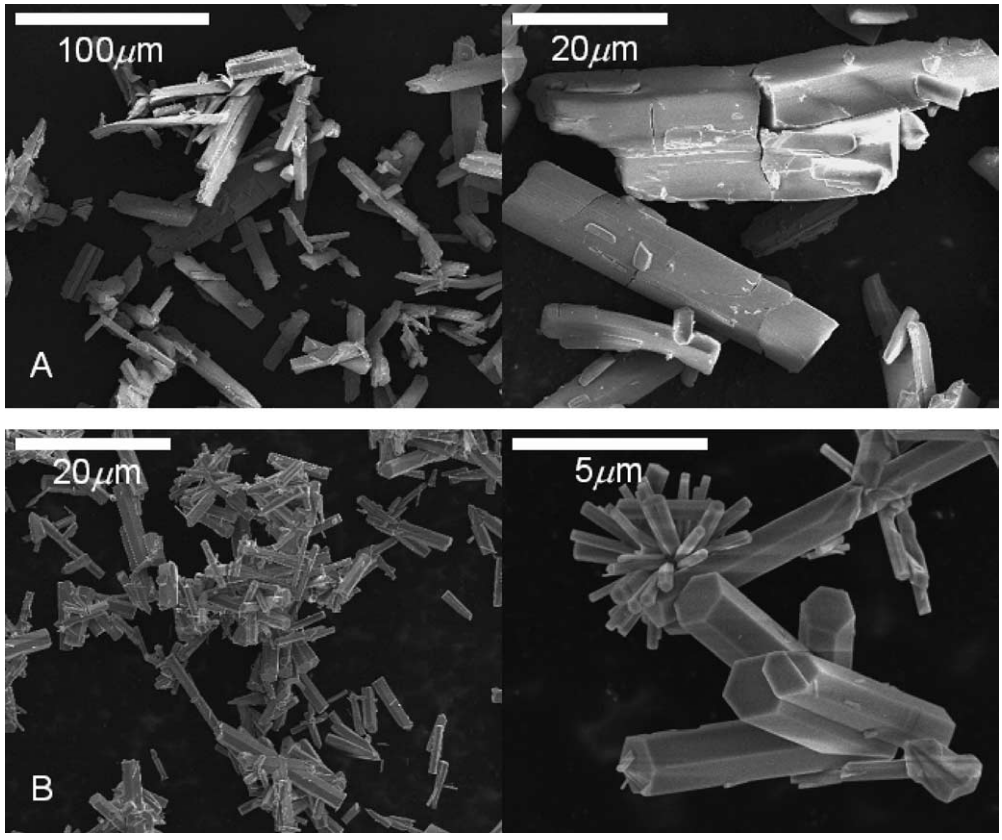

Fig. 4. Typical SEM images of sample 1 (A) and sample 2 (B). Corresponding EDX spectra are absent of impurities. See text for further details.

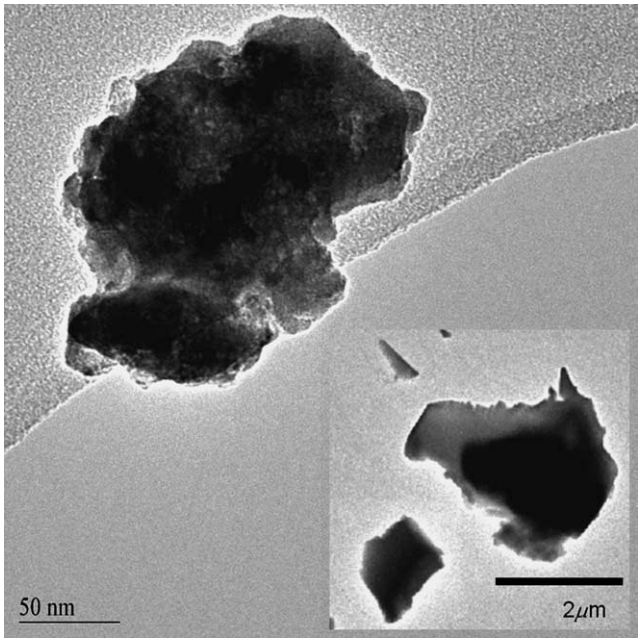

Fig. 5. Low magnification TEM images of sample 1. The smaller particles in the sample have a platelet-like morphology.

from the images. However in the present case the crystal show a long-range periodicity, suggesting large unit-cell parameters. Furthermore, agglomerates of crystals exhibiting well-ordered lattice fringes in ranges of about 10 nm in diameter are observed in sample 1. A characteristic lattice fringe image of such an agglomerate is shown in Fig. 7. The crystals are embedded in a disordered structure, as emphasized with a circle in Fig. 7. This disordered structure might work as a binder for the nanostructured material. The typical distance of 0.38 nm between the lattice fringes in the images is characteristic of layers of molybdenum oxide octahedra. The surface termination of the crystal agglomerate in the main image seems to be disordered. The agglomerate is made from nanocrystals consisting of regular stacks of Mo octahedra with irregular in-plane ordering. Individual layers or clusters of these Mo-octahedra sheets cover part of the surface of the crystals. In view of the fact that the crystal structure according to lattice fringe images does not match a known phase it is difficult to give directions of projections or to describe the structure more in detail.

Sample 2 exhibits a close similarity between the mesoscopic habitus of the SEM image in Fig. 4 and the microstructure being also composed of lamellae with sharp or rounded edges as showed in the inset of Fig. 8. The main image in Fig. 8 shows a lattice fringe image of sample 2. The pronounced lattice spacing in the image is 0.35 nm with a mutual angle of 80° as revealed from FFT analysis. From the lattice fringe images acquired from the sample it is not possible to uniquely determine the structure. However, the structure revealed in Fig. 8 does not match the structure of the hexagonal phase of molybdenum oxide. The darker fringes, which are separated with a distance of ca. 2 nm,

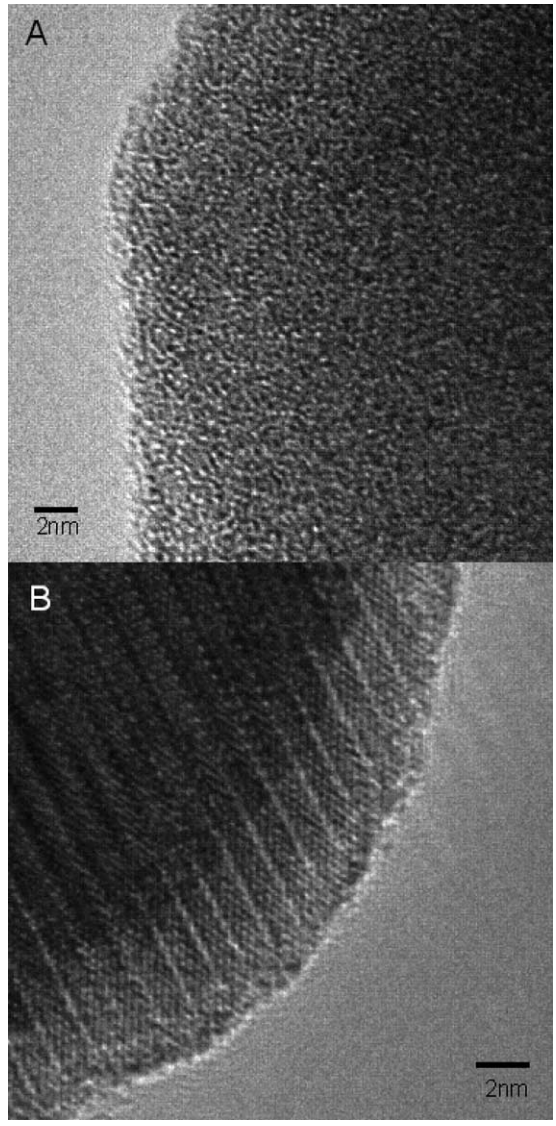

Fig. 6. High magnification TEM images of sample 1. (A) Amorphous part of the sample. (B) Image of big crystal showing clear lattice fringes.

might be due to thickness variation resulting from a layered structure perpendicular to the beam. An amorphous arrangement of material is observed at the corner of the big single crystal as well, as the crystal edges are covered with a 1-nm-thick noncrystalline structure.

Fig. 9 reveals another lattice fringe image of sample 2. The lattice fringe distances corresponding to the main features calculated from FFT analysis are 0.67 and 0.44 nm perpendicular to each other. This does not match the structure of hexagonal molybdenum oxide. It is worth noting that the structure of these single crystals of up to 50 nm in size is not resolved in the XRD measurements. An amorphous or disordered layer of about 2 nm thickness forms the termination of the crystal.

Lattice fringe images are projections; hence significant internal disorder in the direction parallel to the electron beam leads to the variation in contrast along the lattice fringes

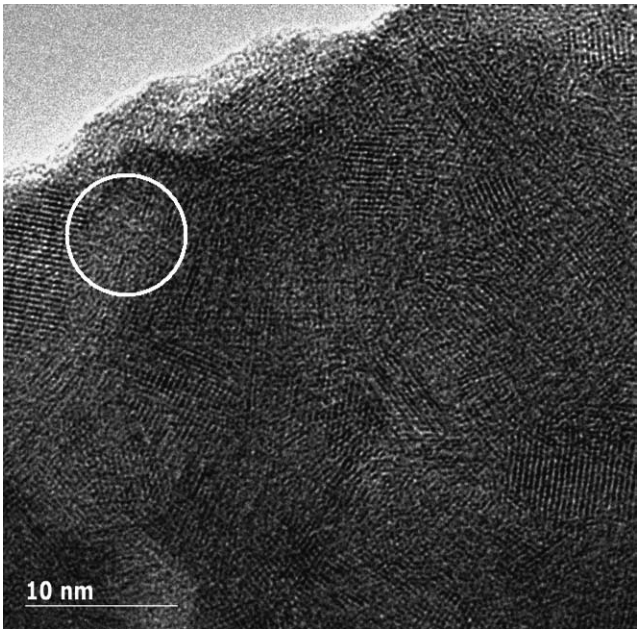

Fig. 7. Lattice fringe image of sample 1 showing agglomerate of nanocrystals. The typical distance between the fringes is 0.38 nm—characteristic of layers of molybdenum oxide octahedra. The circle emphasizes the noncrystalline structure, which embeds the nanocrystals.

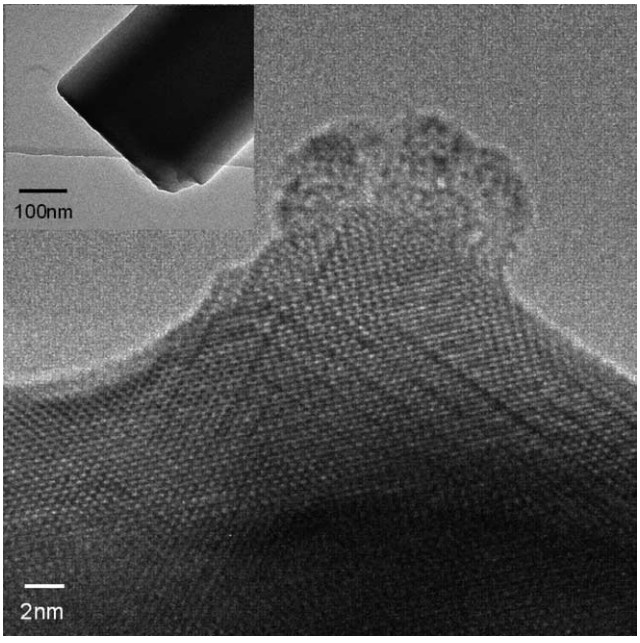

Fig. 8. TEM of sample 2. The main image shows a lattice fringe image of a single crystal. The inset is a TEM image showing the well-defined big particles.

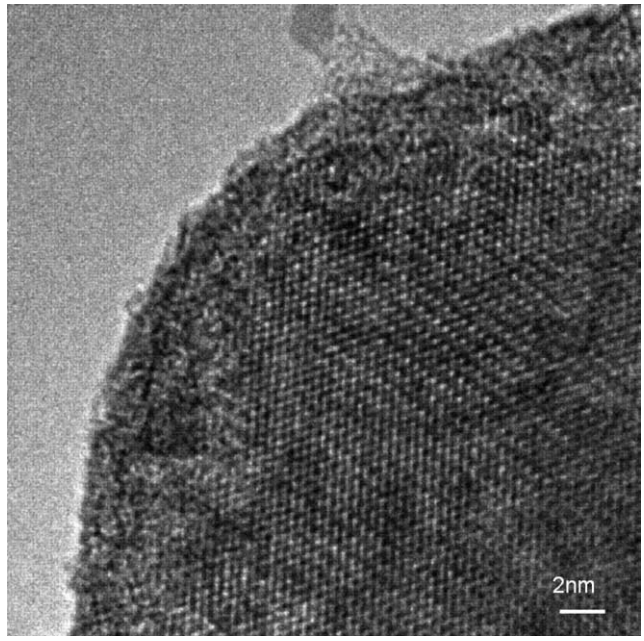

Fig. 9. Lattice fringe image of sample 2. The crystalline structure, which does not match hexagonal Mo oxide, is embedded by a 2-nm disordered layer.

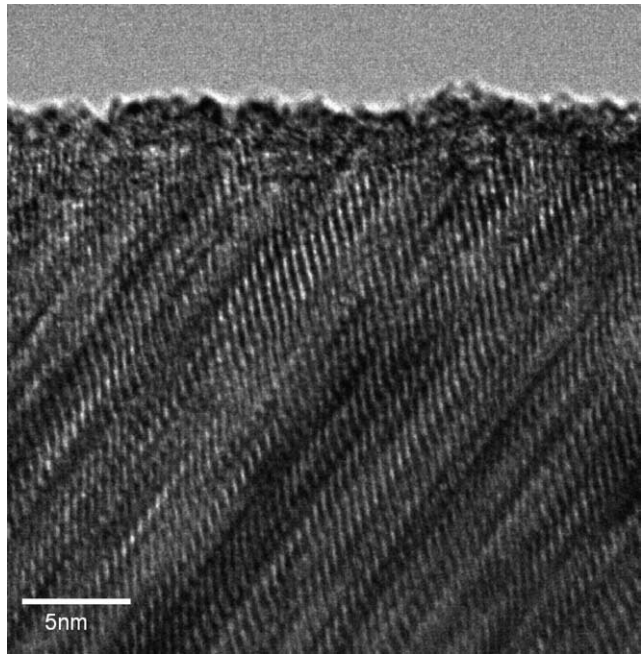

Fig. 10. Lattice fringe image of sample 2 showing fringes, which may indicate the twisted bundles forming the wall in the hexagonal channel structure.

under suitable microscope conditions. The fringes are frequently not exactly parallel but form twisted bundles as displayed in Fig. 10. The pronounced fringes in vertical direction are locally variable with distances between 0.36 and 0.38 nm. They might represent the double block octahedral units making the walls of the hexagonal channel structure [26]. Again a disordered layer of about 2 nm is observed to cover the crystal.

It is remarkable that even at this level of spatial resolution the sample that is apparently single-phase from XRD is not composed of one phase only.

4. Discussion

It is commonly assumed that selective oxidation catalysts either must be supported or must be chemically more complex than a binary oxide to fulfil the requirement of site isolation indispensably connected to selective oxidation [2,27]. From kinetic studies it was further derived that two types of oxygen species (nucleophilic and electrophilic) are competing for organic intermediates and so explain the selectivity patterns of partial oxidation [28]. Bulk o-Mo should, according to these statements and the findings in the literature [12,13], be an unsuitable selective oxidation catalyst. The present data show, however, that significant catalytic performance in propene oxidation is achieved over alkali-free, unsupported metastable varieties of molybdenum oxide obtained from hydrated polymers of MoO_6 octahedra. Both types of materials used here are precursors to a metastable unidentified structure different from o-Mo. The system exhibits chemical memories as they remember the nature of the precursor.

The phase identification and hence a detailed structural study of the phenomenon are severely hampered by the fact that large and small objects on the nanoscale exhibit pronounced structural differences as revealed by the disagreement between X-ray diffraction and electron diffraction probing different size scales of the material. It remains speculative whether different degrees of hydration or different concentrations of the structure-directing ammonium ions can explain the structural differences.

Both samples exhibit pronounced nanostructuring that is not obvious in X-ray diffraction (well-defined powder patterns). The nanostructuring is a precondition for facilitating the structural transformation given that the samples are precursors to a metastable active binary oxide. In conventional calcination up to 773 K the nanostructuring is lost for the growth of large crystals of o-Mo that cannot undergo structural transformations unless chemical reduction and oxygen self-diffusivity [29] sets in [19,20]. The apparently essential operation of “lattice oxygen” may find an alternative explanation as indicator for the structural dynamics of the oxide required to form the metastable active phase.

Structure–activity correlations conducted with the complex MMO phases [30–34] all assume that bulk and surface structures of the phases are well-known and static even in their compositional disorder. The studies identify “synergy” between highly crystalline materials as a key issue. The present TEM images revealing the complex termination of nominally simple binary oxides indicate alternative explanations for the nonobvious quantitative correlations between phase composition and catalytic function. The appeal of disorder seen in the TEM images at surfaces is not necessarily an indication of an amorphous nature of the surface layer. In any oblique projection, complex structures will look disordered. It is, however, plausible that a mixture of tetrahedral and higher coordinated Mo polyhedra is essential [10,35] for a well functioning of the catalyst, taking into account the functional knowledge derived from supported Mo-oxide catalysts. As such motifs are not typical either for the known bulk structures discussed here or for the crystalline M1 and M2 phases it should be assumed that structural rearrangements at the surface during activation may occur. The active system in supported systems [11,36] and in the MMO systems may be similar with the bulk Mo oxides serving as self-support for a disordered surface layer. The higher activity for lower temperatures of sample 1 compared to sample 2 may be seen in this light. The disordered structure observed by TEM to embed the clusters in sample 1 enhances the structural mobility toward self-supported oxides in contrast to the more rigid structure of larger crystals observed in sample 2. However, for in-depth studies of the structural development during catalytic activation, environmental in situ TEM is necessary. The notion that structural dynamics is essential for a good catalyst precursor that manifests itself in the present finding is also conveyed in the literature reports on MMO systems about the pronounced sensitivity of the chemical function on minute kinetic details of the preparation and activation procedures [7,37]. Synergy between phases may thus be an indicator for the readiness for structural dynamics or be the consequence of phase separation from the active metastable material upon removal from the operating conditions. The *additives* to MoO_3 as the foreign species in Mo-based MMO were termed in the literature [8] would then enable the structural dynamics and stabilize metastable Mo–oxo clusters that are the essential carriers of the catalytic activity. The involvement of additive species in mechanistic scenarios of propene oxidation is not necessary [2].

The structural concept of active Mo clusters with, e.g., tetrahedral linkers was put forward with the Mo–V oxides [38] and is confirmed by the present finding of the nonessential role of cationic additives to structurally complex single cationic catalysts. In this way the present images of a nanostructured oxide with a disordered or glassy surface termination (see Figs. 6–10) are a still static illustration of the concept of a dynamical or breathing surface of a selective oxidation catalyst [12,39]. The present findings underline that surface-sensitive in situ studies are essential for investigating the physical origin of phase cooperation and synergy found as phenomenological concepts in MMO catalysts. Toward this end the availability of the present chemically simple functional systems is essential for method development and calibration.

5. Conclusions

Binary Mo-oxide can be an effective selective oxidation catalyst. This holds at least for olefin oxidation. Its extension to alkane activation is presently under study. The work reveals that chemical complexity claimed to be essential for selective oxidation catalysts is not necessary if the catalysts exhibits the necessary structural complexity. This complex-

ity is higher than that provided by o-Mo in well-crystalline form. As this complexity is, however, clearly beneficial for the practical performance it is concluded that controlling and preservation of the nanostructure of the active phase may be key roles of the additive species. This opens the avenue for the preparation of chemically simpler catalysts with more suitable synthetic procedures than precipitation and calcination yielding the matrix and the defective active phase. The investigation of highly crystalline materials for functional analysis of selective oxidation catalysts should be considered with great reservation as such systems do not cover the nanostructural details that were found to be essential for catalytic function.

Acknowledgment

The authors thank G. Weinberg for the SEM work.

References

[1] M.M. Lin, Appl. Catal. A 207 (2001) 1–16.
[2] R.K. Grasselli, Top. Catal. 21 (2002) 79–88.
[3] R.K. Grasselli, Top. Catal. 15 (2001) 93–101.
[4] D.L. Stern, R.K. Grasselli, J. Catal. 167 (1997) 550–559.
[5] S. Knobl, G.A. Zenkovets, G.N. Kryukova, O. Ovsitser, D. Niemeyer, R. Schlogl, G. Mestl, J. Catal. 215 (2003) 177–187.
[6] J. Haber, E. Lalik, Catal. Today 33 (1997) 119–137.
[7] M.M. Lin, Appl. Catal. A 250 (2003) 305–318.
[8] B. Grzybowska, Top. Catal. 21 (2002) 35–46.
[9] K. Chen, S. Xie, A.T. Bell, E. Iglesia, J. Catal. 198 (2001) 232–242.
[10] K.D. Chen, A.T. Bell, E. Iglesia, J. Phys. Chem. B 104 (2000) 1292–1299.
[11] R. Radhakrishnan, C. Reed, S.T. Oyama, M. Seman, J.N. Kondo, K. Domen, Y. Ohminami, K. Asakura, J. Phys. Chem. B 105 (2001) 8519–8530.
[12] J.C. Vedrine, Top. Catal. 21 (2002) 97–106.
[13] G. Mestl, J. Raman Spectrosc. 33 (2002) 333–347.
[14] K.H. Tytko, G. Baethe, E.R. Hirschfeld, K. Mehmke, D. Stellhorn, Z. Anorg. Allg. Chem. 503 (1983) 43–66.
[15] K.H. Tytko, O. Glemser, Adv. Inorg. Chem. Radiochem. 19 (1976) 239.
[16] A. Müller, A. Beckmann, H. Bögge, M. Schmidtmann, A. Dress, Angew. Chem. 114 (2002) 1210–1215.
[17] S.B. Abd Hamid, D. Othman, N. Abdullah, O. Timpe, S. Knobl, D. Niemeyer, J. Wagner, D. Su, R. Schlogl, Top. Catal. 24 (2003) 87–95.
[18] T. Ressler, O. Timpe, T. Neisius, J. Find, G. Mestl, M. Dieterle, R. Schlogl, J. Catal. 191 (2000) 75–85.
[19] T. Ressler, J. Wienold, R.E. Jentoft, F. Girgsdies, Eur. J. Inorg. Chem. (2003) 301–312.
[20] T. Ressler, J. Wienold, R.E. Jentoft, T. Neisius, J. Catal. 210 (2002) 67–83.
[21] B. Bems, M. Schur, A. Dassenoy, D. Herein, R. Schlögl, Chem. Eur. J. 9 (2003) 2039–2052.
[22] T. Ilkenhans, B. Herzog, T. Braun, R. Schlögl, J. Catal. 153 (1995) 275–292.
[23] G. Mestl, T. Ilkenhans, D. Spielbauer, M. Dieterle, O. Timpe, J. Krohnert, F. Jentoft, H. Knozinger, R. Schlogl, Appl. Catal. A 210 (2001) 13–34.
[24] B. Krebs, I. Paulat-Böschen, Acta Crystallogr. B 38 (1982) 1710–1713.
[25] S. Berndt, D. Herein, F. Zemlin, E. Beckmann, G. Weinberg, J. Schutze, G. Mestl, R. Schlogl, Ber. Bunsen-Ges. Phys. Chem. 102 (1998) 763–774.
[26] O. Mougin, J.L. Dubois, F. Mathieu, A. Roussett, J. Solid State Chem. 152 (2000) 353–360.
[27] R.K. Grasselli, J.D. Burrington, Adv. Catal. 30 (1981) 133–163.
[28] J. Haber, W. Turek, J. Catal. 190 (2000) 320–326.
[29] R. Kapoor, S.T. Oyama, J. Mater. Res. 12 (1997) 467–473.
[30] P. DeSanto, D.J. Buttrey, R.K. Grasselli, C.G. Lugmair, A.F. Volpe, B.H. Toby, T. Vogt, Top. Catal. 23 (2003) 23–38.
[31] R.K. Grasselli, J.D. Burrington, D.J. Buttrey, P. DeSanto, C.G. Lugmair, A.F. Volpe, T. Weingand, Top. Catal. 23 (2003) 5–22.
[32] J. Holmberg, R.K. Grasselli, A. Andersson, Top. Catal. 23 (2003) 55–63.
[33] M. Baca, A. Pigamo, J.L. Dubois, J.M.M. Millet, Top. Catal. 23 (2003) 39–46.
[34] J.N. Al Saeedi, V.K. Vasudevan, V.V. Guliants, Catal. Commun. 4 (2003) 537–542.
[35] K.D. Chen, S.B. Xie, E. Iglesia, A.T. Bell, J. Catal. 189 (2000) 421–430.
[36] A.N. Desikan, W.M. Zhang, S.T. Oyama, J. Catal. 157 (1995) 740–748.
[37] E.K. Novakova, J.C. Vedrine, E.G. Derouane, J. Catal. 211 (2002) 235–243.
[38] H. Werner, O. Timpe, D. Herein, Y. Uchida, N. Pfänder, U. Wild, R. Schlögl, Catal. Lett. 44 (1997) 153–163.
[39] J.C. Vedrine, E.K. Novakova, E.G. Derouane, Catal. Today 81 (2003) 247–262.